Geotechnical Testing Journal

doi:10.1520/GTJ20170313 / Vol. 42 / No. 3 / 2019 / available online at www.astm.org

Amin Soltani,[1] An Deng,[2] Abbas Taheri,[2] and Asuri Sridharan[3]

Swell–Shrink–Consolidation Behavior of Rubber–Reinforced Expansive Soils

Reference

Soltani, A., Deng, A., Taheri, A., and Sridharan, A., "Swell–Shrink–Consolidation Behavior of Rubber–Reinforced Expansive Soils," *Geotechnical Testing Journal*, Vol. 42, No. 3, 2019, pp. 761–788, https://doi.org/10.1520/GTJ20170313. ISSN 0149-6115

ABSTRACT

This study examines the effects of two types of recycled tire rubber of fine and coarse categories on the swell–shrink–consolidation behavior of a highly expansive soil mixture. Each of the two rubber choices were incorporated into the soil at four different content levels (i.e., rubber to dry soil mass ratio) of 5, 10, 20, and 30 %. The experimental program consisted of consistency limits, compaction, swell–consolidation, swell–shrink, and unconfined compression tests. Improvement in the swell–shrink–consolidation capacity was in favor of higher rubber contents; however, when excessively included, it raised strength concerns. The swell–shrink–consolidation properties were also rubber size-dependent, meaning that the rubber of coarser sizes often outperformed finer rubber. In terms of strength, however, the two rubber types promoted similar results with marginal differences. The results of the unconfined compression tests were cross checked with the swell–shrink–consolidation properties to arrive at the optimum stabilization scenarios. A maximum rubber inclusion of 10 %, preferably the rubber of coarser category, proved to satisfy the stabilization objectives (i.e., decrease in the swell–shrink–consolidation capacity as well as maintain or improve the strength) and thus was deemed as the optimum choice. Where context changes and the strength and stiffness are not a primary concern, higher rubber inclusions of up to 20 % may also be considered acceptable.

Keywords

expansive soils, recycled tire rubbers, rubber content and size, swell–shrink–consolidation, unconfined compression

Manuscript received September 8, 2017; accepted for publication March 26, 2018; published online August 28, 2018.

[1] School of Civil, Environmental and Mining Engineering, The University of Adelaide, North Terrace, SA 5005, Australia (Corresponding author), e-mail: Amin.Soltani@adelaide.edu.au, https://orcid.org/0000-0002-0483-7487

[2] School of Civil, Environmental and Mining Engineering, The University of Adelaide, North Terrace, SA 5005, Australia

[3] Indian National Science Academy, New Delhi 110002, India; Department of Civil Engineering, Indian Institute of Science, CV Raman Rd, Bangalore 560012, India (retired)

Introduction

Expansive soils are low graded because of their inferior engineering characteristics (e.g., low strength, high compressibility, and a high potential for swelling and shrinkage), and thus are characterized as unsuitable construction materials for the majority of engineering applications (Dif and Bluemel 1991; Nalbantoglu 2006; Estabragh et al. 2013). When exposed to seasonal environments, such soils are prone to significant volume changes, i.e., heave and settlements, thereby causing instability concerns to the overlying structures. Such concerns incur a great amount of maintenance costs and therefore demand engineering solutions to alleviate the associated socioeconomic impacts on human life (Jones and Jefferson 2012). Stabilization of expansive soils is often achieved through two approaches, i.e., chemical and mechanical techniques (Winterkorn and Pamukcu 1991). Chemical techniques mainly involve the addition of chemical binders, such as traditional cement, lime, and fly ash or nontraditional polymers, sulfonated oils, resins, and enzymes, to the soil mass, thereby amending the soil fabric into a coherent matrix of restricted heave/settlement and induced strength (e.g., Al-Rawas, Hago, and Al-Sarmi 2005; Mirzababaei, Yasrobi, and Al-Rawas 2009; Thyagaraj and Zodinsanga 2014; Onyejekwe and Ghataora 2015; Alazigha et al. 2016; Jha and Sivapullaiah 2016; Soltani et al. 2017a). The mechanical approach makes use of compaction with the aid of reinforcements. Conventional reinforcements include fibers of synthetic (e.g., polypropylene, steel, and nylon) or natural (e.g., coir and palm) origin (e.g., Cai et al. 2006; Al-Akhras et al. 2008; Viswanadham, Phanikumar, and Mukherjee 2009a, 2009b; Mirzababaei et al. 2013a; Olgun 2013; Estabragh, Rafatjo, and Javadi 2014; Estabragh, Soltani, and Javadi 2016; Phanikumar and Singla 2016; Shahbazi et al. 2017; Mirzababaei et al. 2017, 2018; Soltani, Deng, and Taheri 2018). As the global community shifts toward a more sustainable mindset, alternate stabilization techniques capable of replacing or minimizing the use of such conventional agents have been highly encouraged. Beneficial reuse of solid waste materials and industrial byproducts may be regarded amongst the most well-received propositions in this context. The proposition not only addresses the expansive soil problem, but also offers a sound solution to minimizing the environmental impacts associated with waste materials.

Discarded tires have become an ongoing environmental crisis, particularly in industrialized countries where tire stockpiles have reached alarming volumes. In Australia, for instance, it is estimated that 48 million tires are disposed of each year, signifying a relative abundance of waste tires available for beneficial reuse (Hannam 2014). Waste tires have excellent mechanical properties (e.g., durability, resiliency, and frictional resistance), which suggests that they are an attractive material for geotechnical applications, such as soil stabilization (Zornberg, Cabral, and Viratjandr 2004). Similar to fiber–reinforced soils, the rubber assemblage randomly distributes in the soil regime, and where optimized in dosage and geometry, could potentially ameliorate the expansive soil with respect to moisture sensitivity (i.e., swell–shrink-related volume changes), compressibility, strength, and ductility (e.g., Edil and Bosscher 1994; Cetin, Fener, and Gunaydin 2006; Akbulut, Arasan, and Kalkan 2007; Seda, Lee, and Carraro 2007; Özkul and Baykal 2007; Dunham-Friel and Carraro 2011; Garcia, Pando, and Tempest 2011; Patil, Valdes, and Evans 2011; Trouzine, Bekhiti, and Asroun 2012; Kalkan 2013; Srivastava, Pandey, and Rana 2014; Signes et al. 2016; Yadav and Tiwari 2017). As such, the rubber reinforcement mechanism is expected to be primarily a function of rubber content. However, the rubber's

geometrical properties, hereafter referred to as rubber size, could also portray an equally important role in yielding an effective stabilization scheme. The latter should be somewhat similar to the aspect ratio (i.e., fiber length to diameter ratio) in fiber–reinforced soils, which has been well documented in the aforementioned fiber reinforcement literature (e.g., Estabragh, Rafatjo, and Javadi 2014; Phanikumar and Singla 2016; Soltani, Deng, and Taheri 2018). With rubbers, however, this aspect has not yet been adequately addressed in the literature (e.g., Cetin, Fener, and Gunaydin 2006; Srivastava, Pandey, and Rana 2014) in what can describe the rubber reinforcement technique as an ad hoc stabilization solution demanding further examination.

To address the uncertainties associated with selecting effective soil–rubber proportions, this study intends to evaluate the effect of two types of recycled tire rubber of fine and coarse category on the swell–shrink–consolidation behavior of a highly expansive soil mixture. A series of unconfined compression (UC) tests was also carried out, and the results were cross checked with the swell–shrink–consolidation properties to arrive at the optimum stabilization scenarios.

Materials and Methods

EXPANSIVE SOIL

Commercially available kaolinite and bentonite were used for this study. A mixture of 85 % kaolinite and 15 % bentonite was selected as the expansive soil for further experimental work. This mixture, hereafter simply referred to as soil, was characterized as "clay with high plasticity" (CH) in accordance with the Unified Soil Classification System (USCS). The mechanical properties of kaolinite, bentonite, and the kaolinite–bentonite mixture, determined as per relevant ASTM or Australian standards, are summarized in **Table 1**. The chemical compositions of the kaolinite and bentonite, as supplied by the manufacturer, are provided in **Table 2**. The free swell ratio for kaolinite, bentonite, and the

TABLE 1

Mechanical properties of kaolinite, bentonite, and the expansive soil.

Properties	Kaolinite	Bentonite	Expansive Soil	Standard Designation
Specific gravity, G_s	2.68	2.81	2.73	ASTM D854 (2014)[a]
Clay (<2 μm) (%)	49.78	62.43	N/A[b]	ASTM D422 (2007)[c]
Silt (2–75 μm) (%)	49.43	35.75	N/A	ASTM D422 (2007)
Sand (0.075–4.75 mm) (%)	0.79	1.82	N/A	ASTM D422 (2007)
Liquid limit, *LL* (%)	41.04	379.21	59.60	AS 1289.3.9.1 (2015)[d]
Plastic limit, *PL* (%)	23.67	45.18	27.28	AS 1289.3.2.1 (2009)[e]
Plasticity index, *PI* (%)	17.37	334.03	32.32	AS 1289.3.3.1 (2009)[f]
Free swell ratio, *FSR*[g]	1.19	7.53	2.91	Prakash and Sridharan (2004)
USCS classification	CI	CH	CH	ASTM D2487 (2011)[h]
Optimum water content, ω_{opt} (%)	19.82	36.34	26.00	ASTM D698 (2012)[i]
Maximum dry unit weight, γ_{dmax} (kN/m^3)	15.67	11.74	15.07	ASTM D698 (2012)

Note: [a]ASTM D854, *Standard Test Methods for Specific Gravity of Soil Solids by Water Pycnometer*; [b]not measured; [c]ASTM D422, *Standard Test Method for Particle–Size Analysis of Soils*; [d]AS 1289.3.9.1:15, *Methods of Testing Soils for Engineering Purposes: Soil Classification Tests–Determination of the Cone Liquid Limit of a Soil*; [e]AS 1289.3.2.1:09, *Methods of Testing Soils for Engineering Purposes: Soil Classification Tests–Determination of the Plastic Limit of a Soil*; [f]AS 1289.3.3.1:09, 2009, *Methods of Testing Soils for Engineering Purposes: Soil Classification Tests–Calculation of the Plasticity Index of a Soil*; [g]ratio of equilibrium sediment volume of 10 gr oven-dried soil passing sieve 425 μm in distilled water to that of kerosene; [h]ASTM D2487, *Standard Practice for Classification of Soils for Engineering Purposes (Unified Soil Classification System)*; [i]ASTM D698, *Standard Test Methods for Laboratory Compaction Characteristics of Soil Using Standard Effort (12,400 ft–lbf/ft^3 (600 kN–m/m^3))*.

TABLE 2

Chemical composition of kaolinite and bentonite (as supplied by the manufacturer).

Properties	Kaolinite	Bentonite
SiO_2 (%)	64.9	63.2
Al_2O_3 (%)	22.2	13.3
TiO_2 (%)	1.4	0.3
Fe_2O_3 (%)	1.0	2.6
CaO (%)	0.1	0.3
Na_2O (%)	0.2	1.9
MgO (%)	0.6	2.2
K_2O (%)	2.7	0.2
Acidity, pH	7.4	9.5
LOI at 1,000°C (%)[a]	6.5	16.0
CEC (meq/100mL)[b]	N/A[c]	82
SSA (m^2/gr)[d]	11.2	N/A

Note: [a]loss on ignition; [b]cation exchange capacity; [c]not available; [d]specific surface area.

kaolinite–bentonite mixture was 1.19, 7.53, and 2.91, from which these soils were graded into "lowly expansive," "very highly expansive," and "highly expansive" with respect to the classification criteria proposed by Prakash and Sridharan (2004), respectively.

TIRE RUBBERS

Two types of commercially available recycled tire rubber, commonly traded as rubber crumbs and rubber buffings (a byproduct of the tire retreading process), were used as reinforcements. Hereafter, these rubber types will be referred to as Rubbers A and B, respectively. The grain size distribution curves for kaolinite, bentonite, and Rubbers A and B, determined as per ASTM D422, *Standard Test Method for Particle–Size Analysis of Soils*, are shown in Fig. 1. Rubber A can be assumed to be similar in size to fine sand, having an average particle size ranging between 1.18 mm and 75 μm ($d_{50} = 0.478$ mm). Rubber B, however, falls into the coarse sand category, having an

FIG. 1

Grain size distribution curves for kaolinite, bentonite, and the tire rubbers.

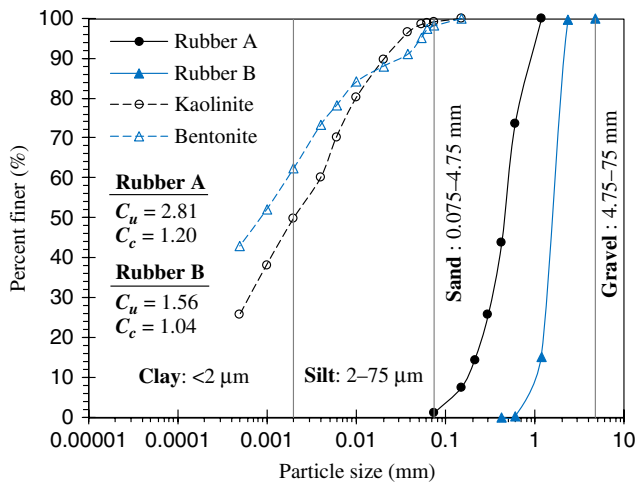

TABLE 3
Physical properties and chemical composition of the tire rubbers (as supplied by the manufacturer).

Properties	Value
Physical Properties	
Solubility in water	Insoluble
Water adsorption	Negligible
Resistance to acid and alkaline	Excellent
Specific gravity at 20°C	1.09
Particle size for Rubber A (mm)	1.18–0.075
Particle size for Rubber B (mm)	4.75–1.18
Softening point (°C)	170
Chemical Composition	
Styrene–butadiene copolymer (%)	55
Acetone extract (%)	5–20
Carbon black (%)	25–35
Zinc oxide (%)	2.5
Sulphur (%)	1–3

average particle size ranging between 4.75 and 1.18 mm ($d_{50} = 1.582$ mm). Both rubber types can be classified as poorly graded sand or SP (in accordance with USCS) corresponding to uniformity and curvature coefficients of $C_u = 2.81$ and $C_c = 1.20$ for Rubber A, and $C_u = 1.56$ and $C_c = 1.04$ for Rubber B. Each of the two rubber choices were incorporated into the soil at four different contents (defined as rubber to dry soil mass ratio), i.e., $R_c = 5$, 10, 20, and 30 %. The physical and chemical properties, as supplied by the manufacturer, along with a photograph (to scale) of the rubber particles are provided in Table 3 and Fig. 2, respectively.

SPECIMEN PREPARATION

A series of standard Proctor compaction tests were carried out on the natural soil and various soil–rubber mixtures in accordance with ASTM D698-12e2, *Standard Test Methods for Laboratory Compaction Characteristics of Soil Using Standard Effort (12,400 ft–lbf/ft^3 (600 kN–m/m^3))*, and the results are provided in Fig. 3a and b for Rubbers A and B, respectively. The specific gravity of soil–rubber mixtures, as shown in Fig. 3, was estimated by the theoretical relationship proposed by Trouzine, Bekhiti, and Asroun (2012). Rubber reinforcement led to a noticeable decrease in both the optimum water content ω_{opt} and the maximum dry unit weight γ_{dmax} (see the compaction paths in Fig. 3). The compaction behavior, however, was observed to be independent from the rubber size. Decrease in ω_{opt} and γ_{dmax} can be attributed to the lower specific gravity, specific surface area and water adsorption capacity of rubber particles compared to soil grains (Özkul and Baykal 2007; Kalkan 2013; Signes et al. 2016).

Specimens for the swell–shrink–consolidation test (see section under the "Swell–Shrink–Consolidation Test" heading) were prepared by the static compaction technique at dry of optimum condition (i.e., $\omega_0 = \omega_{opt}$–5 % and its corresponding dry unit weight γ_{d0}). The required amount of water corresponding to the desired water content (see ω_0 in Table 4) was added to each mixture and thoroughly mixed by hand. Extensive care was dedicated to pulverizing the lumped particles, targeting homogeneity of mixtures. Mixtures were then enclosed in plastic bags and stored under room temperature conditions for 24 hours, ensuring even distribution of moisture throughout the soil mass.

FIG. 2

Tire rubbers at 50× magnification: (a) Rubber A and (b) Rubber B.

(a)

(b)

A special split mold, similar to that described in Soltani et al. (2017b), was designed and fabricated from stainless steel to accomplish static compaction. The mold consisted of three sections, i.e., the top collar, the middle oedometer ring, and the bottom collar. The oedometer ring measures 50 mm in diameter and 20 mm in height, and it accommodates the specimen for the swell–shrink–consolidation test. The mixtures were gradually compressed in the mold in three layers to a specific compaction load, each layer having attained the target dry unit weight (see γ_{d0} in Table 4). The inner surface of the mold was smeared with a thin layer of silicon grease to avoid friction during compaction. The surface of the first and second compacted layers were scarified to ensure a good bond between adjacent layers of the mixture. Specimens for the UC test (see the section under the "UC Test" heading) were prepared in a similar fashion. In this case, however, a different mold, resulting in specimens measuring 50 mm in diameter and 100 mm in height, along with five compaction layers was adopted. In addition, the UC specimens were prepared at optimum condition (see ω_{opt} and $\gamma_{d\max}$ in Table 4). Mechanical properties of the prepared specimens, including the consistency limits and the initial placement conditions, are summarized in Table 4. For natural soils, the optimum water content ω_{opt} can be estimated by means of the plastic limit PL through $\omega_{opt} = 0.92PL$ (Gurtug and Sridharan 2002, 2004; Sridharan and Nagaraj 2005). Interestingly, the same holds true for various soil–rubber mixtures (see Table 4).

FIG. 3

Standard Proctor compaction curves for the natural soil and various soil–rubber mixtures: (a) Rubber A and (b) Rubber B.

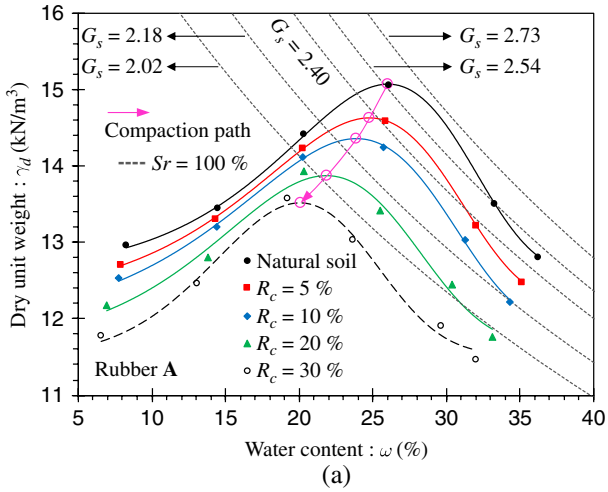

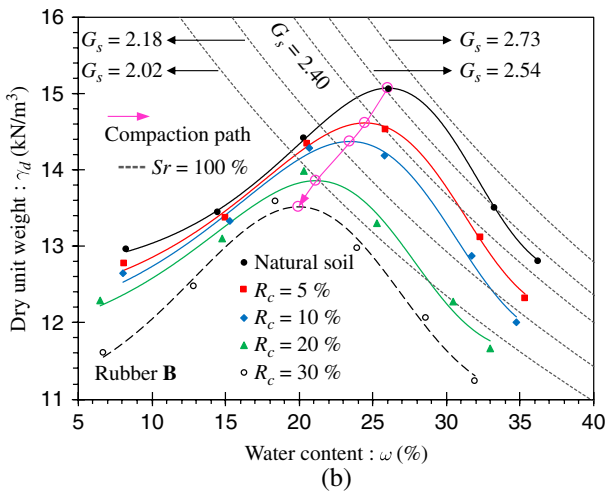

TABLE 4

Mechanical properties of the prepared specimens.

Rubber Type	R_c (%)	G_s	LL (%)	PL (%)	PI (%)	ω_{opt} (%)	0.92PL (%)[a]	γ_{dmax} (kN/m^3)	e_{opt}[b]	ω_0 (%)	γ_{d0} (kN/m^3)	e_0[c]
–	0	2.73	59.60	27.28	32.32	26.00	25.10	15.07	0.775	21.00	14.52	0.842
Rubber A	5	2.54	57.03	27.02	30.01	24.77	24.86	14.63	0.706	19.77	14.16	0.763
	10	2.40	55.04	25.54	29.50	23.87	23.50	14.35	0.639	18.87	13.90	0.693
	20	2.18	51.51	23.46	28.05	21.85	21.58	13.87	0.541	16.85	13.40	0.596
	30	2.02	49.58	22.70	26.88	20.07	20.88	13.52	0.469	15.07	12.92	0.537
Rubber B	5	2.54	56.88	26.61	30.27	24.47	24.48	14.61	0.709	19.47	14.15	0.764
	10	2.40	55.62	24.77	30.85	23.46	22.79	14.37	0.638	18.46	13.94	0.689
	20	2.18	52.44	23.27	29.17	21.15	21.41	13.86	0.543	16.15	13.43	0.593
	30	2.02	51.21	22.15	29.06	19.94	20.38	13.52	0.469	14.94	12.99	0.528

Note: [a]predicted optimum water content; [b]initial placement condition for UC tests; [c]initial placement condition for swell–shrink–consolidation tests.

TEST PROCEDURE

Swell–Shrink–Consolidation Test

Specimens were subjected to a series of swell–shrink–consolidation tests. A typical illustration of the test scheme is provided in Fig. 4. The swell–consolidation phase, carried out in accordance with ASTM D4546, *Standard Test Methods for One–Dimensional Swell or Collapse of Soils*, includes two stages, i.e., swell and consolidation. In the first stage, the desired specimen is allowed to freely swell under a low nominal overburden stress of $\sigma'_0 = 1$ kPa. The incurred swelling strain was recorded during various time intervals to a point in which swell–time equilibrium, a state corresponding to the specimen's swelling potential (defined as the ultimate swelling strain), could be achieved (see Path O→A in Fig. 4a). During consolidation, the swollen specimen, now at State A, is gradually loaded to counteract the built-up swelling strain. The stress required to retain the specimen's initial placement or void ratio is taken as the swelling pressure (Sridharan, Rao, and Sivapullaiah 1986). Upon completion of the loading scheme, the specimen is gradually unloaded back to $\sigma'_0 = 1$ kPa (see Path A→B_1 for loading, and Path B_1→C for unloading in Fig. 4b). Test

FIG. 4 A typical illustration of the swell–shrink–consolidation test scheme: (a) swell path, (b) consolidation path, and (c) shrink path.

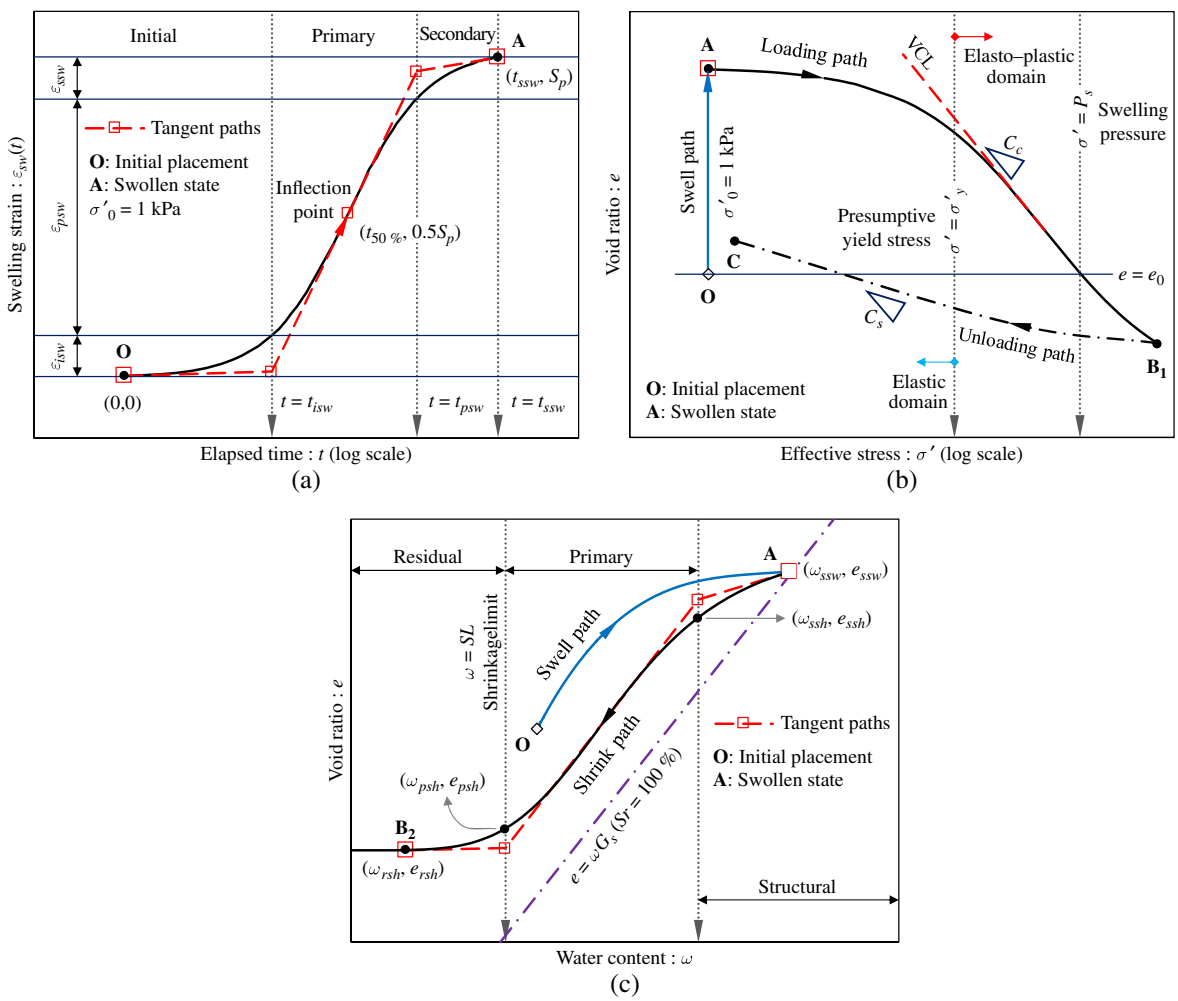

results are presented in the form of swelling strain–time (for the swell stage) and void ratio–effective stress (for the consolidation stage) curves plotted over a semilog space (see Fig. 4a and b, respectively).

The swell–shrink phase also consists of two stages, i.e., swell and shrink. The swell component is essentially similar to that described in the swell–consolidation test. During the shrink stage, the swollen specimen, now at State A, is allowed to desiccate under a constant temperature of 40°C. The volumetric shrinkage strain along with the corresponding water content was directly measured during various time intervals to a point in which shrinkage ceases (see Path A→B_2 in Fig. 4c). The volumetric shrinkage strain was measured by the volume displacement technique outlined in ASTM D427, *Test Method for Shrinkage Factors of Soils by the Mercury Method*, which has also been commonly adopted in the literature (e.g., Sibley and Williams 1989; Hanafy 1991; Subba Rao, Rao, and Gangadhara 2000; Tripathy, Subba Rao, and Fredlund 2002; Tripathy and Subba Rao 2009). For the shrink stage, test results are presented in the form of void ratio–water content curves plotted over an arithmetic space (see Fig. 4c).

UC Test

The UC test was carried out in accordance with ASTM D2166, *Standard Test Method for Unconfined Compressive Strength of Cohesive Soil*. The specimens were compressed by a constant displacement rate of 1 %/min, as commonly adopted in the literature (e.g., Ang and Loehr 2003; Fatahi, Khabbaz, and Fatahi 2012; Signes et al. 2016). To ensure sufficient accuracy, triplicate specimens were tested for each scenario. Axial stress and its corresponding axial strain were recorded during various loading stages to a point in which maximum axial stress required for specimen failure, denoted as q_u, and its corresponding axial strain, denoted as ε_u, could be achieved. The area under the stress–strain curve up to q_u and ε_u—a measure of the material's toughness defined as strain energy at peak E_p (Maher and Ho 1994; Mirzababaei et al. 2013b)—was also obtained for the tested specimens.

Results and Discussion

EFFECT OF RUBBERS ON THE SWELLING POTENTIAL

Swelling strain–time curves, represented by the two-parameter rectangular hyperbola function (e.g., Dakshanamurthy 1978; Sivapullaiah, Sridharan, and Stalin 1996; Sridharan and Gurtug 2004), for the natural soil and various soil–rubber composites are provided in Fig. 5a and b for Rubbers A and B, respectively. As a result of rubber reinforcement, the swelling strain–time locus experienced a major downward shift over the ε_{sw}:log$t$ space (ε_{sw} = swelling strain, and t = time), indicating a significant reduction in the magnitude of exhibited swelling strain, and thus swelling potential (defined as the ultimate swelling strain) compared to the natural soil. At $t = 24$ hours, for instance, the natural soil displayed a swelling strain of $\varepsilon_{sw}(t) = 15.23$ %, while the inclusion of 5, 10, 20, and 30 % Rubber A resulted in $\varepsilon_{sw}(t) = 14.99$, 11.82, 9.01, and 7.67 %, respectively (see Fig. 5a). Similar inclusions of Rubber B, however, exhibited a slightly more pronounced decreasing trend where the above given values dropped to $\varepsilon_{sw}(t) = 13.67$, 11.44, 8.01, and 7.21 %, respectively (see Fig. 5b). The natural soil and soil–Rubber A mixtures corresponding to $R_c = 5$, 10, 20, and 30 % resulted in swelling potential values of $S_p = 18.35$, 16.02, 13.01, 11.17, and 9.56 %, respectively. For similar inclusions of Rubber B, these values further decreased to $S_p = 14.74$, 12.18, 9.02, and 8.11 %, respectively.

FIG. 5

Swelling strain–time curves for the natural soil and various soil–rubber composites: (a) Rubber A and (b) Rubber B.

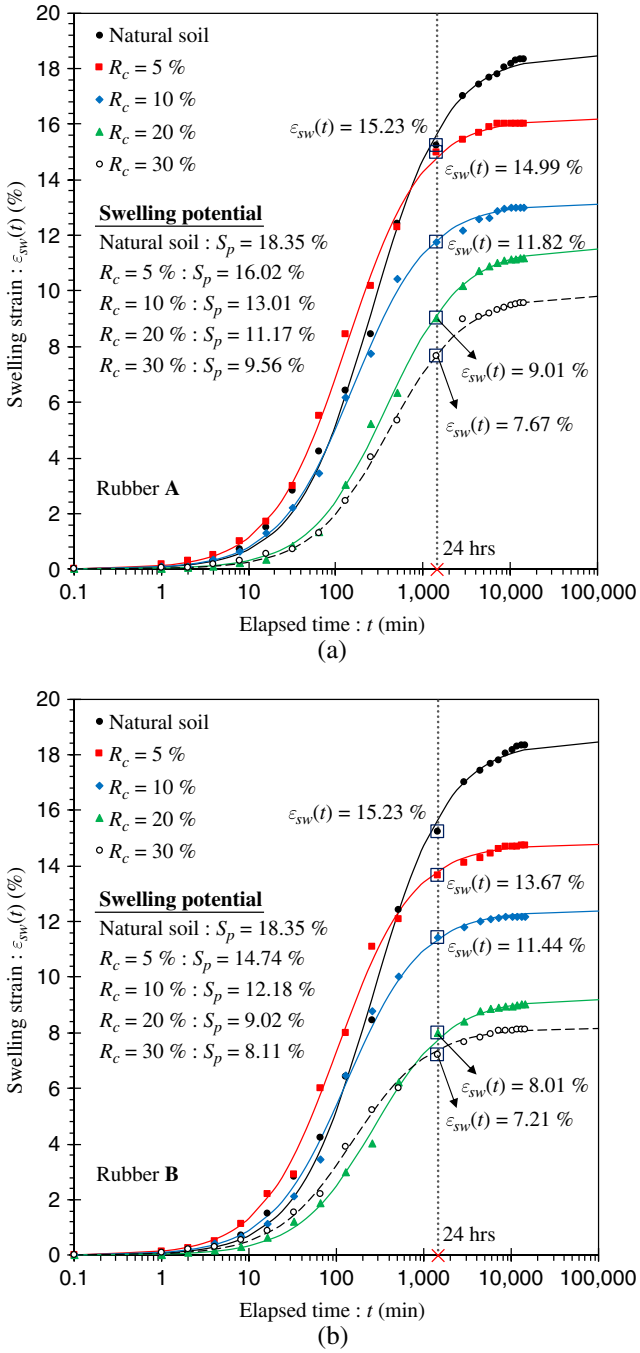

A typical swell path (see Path O→A in Fig. 4a), plotted over a semilog space, develops into an *S*-shaped curve, and thus can be divided into three regions, i.e., the initial, primary, and secondary swelling, which are defined as phases during which swelling takes place (Dakshanamurthy 1978; Sivapullaiah, Sridharan, and Stalin 1996; Sridharan and Gurtug 2004; Rao, Thyagaraj, and Thomas 2006; Soltani et al. 2017b). The initial swelling phase,

also recognized as intervoid or intercrystalline swelling, rapidly evolved at a macrostructural level and is accompanied by small volume changes (i.e., $\varepsilon_{isw} \leq 0.1S_p$). The primary swelling phase constitutes for up to 80 % of the total volume increase (i.e., $\varepsilon_{psw} \approx 0.8S_p$) and is graphically bound by the initial and primary swelling time margins (see Fig. 4a). The secondary swelling phase occurs as a result of double layer repulsion, which results in small time-dependent volume changes. In comparison to initial swelling, both the primary and secondary swelling phases evolve at a microstructural level where the swelling of active minerals takes place. Critical variables obtained from the *S*-shaped swell curve are useful concepts capable of describing the time-dependent nature of the swelling phenomenon under field conditions (Sridharan and Gurtug 2004). These variables, defined by a conventional graphical construction, as depicted in Fig. 4a, can be categorized as follows:

- Completion time of the initial and primary swelling phases, i.e., t_{isw} and t_{psw}.
- Initial, primary, and secondary swelling strains, i.e., ε_{isw}, $\varepsilon_{psw,}$ and ε_{ssw}, where $S_p = \varepsilon_{isw} + \varepsilon_{psw} + \varepsilon_{ssw}$.
- Primary and secondary swelling rates, i.e., C_{psw} and C_{ssw}, which are defined as follows:

$$C_{psw} = \frac{\Delta \varepsilon_{sw}}{\Delta \log t}\Bigg]_{t_{isw}}^{t_{psw}} = \frac{\varepsilon_{psw}}{\log\left(\frac{t_{psw}}{t_{isw}}\right)} \tag{1}$$

$$C_{ssw} = \frac{\Delta \varepsilon_{sw}}{\Delta \log t}\Bigg]_{t_{psw}}^{t_{ssw}} = \frac{\varepsilon_{ssw}}{\log\left(\frac{t_{ssw}}{t_{psw}}\right)} \tag{2}$$

where t_{ssw} = completion time of the secondary swelling phase (≈240 hours).

Fig. 6a and b illustrates the variations of C_{psw} and C_{ssw} against rubber content for the tested specimens, respectively. The rubber inclusions led to a noticeable reduction in C_{psw} and C_{ssw}, indicating a capacity to counteract the heave in both magnitude and time. The greater the rubber content, the greater the decrease in C_{psw} following a monotonic trend. Rubber contents greater than 5 %, however, did not further deviate C_{ssw}. Rubber B consistently outperformed Rubber A by exhibiting lower swelling rates for similar rubber inclusions. The natural soil resulted in $C_{psw} = 8.38 \times 10^{-2}$ and $C_{ssw} = 2.56 \times 10^{-2}$. As a typical case, these values, respectively, dropped to 5.89×10^{-2} and 1.54×10^{-2} for Rubber A, and 5.58×10^{-2} and 1.19×10^{-2} for Rubber B where $R_c = 10$ %.

EFFECT OF RUBBERS ON THE CONSOLIDATION BEHAVIOR

Void ratio–effective stress consolidation curves for the natural soil and various soil–rubber composites are provided in Fig. 7a and b for Rubbers A and B, respectively. A typical consolidation curve with respect to the loading stage (see Path A→B_1 in Fig. 4b), plotted over a semilog space, develops into a two-segment curvilinear relationship and thus can be divided into two regions, i.e., the elastic and elastoplastic compression, which are defined as phases during which consolidation takes place (Sridharan, Abraham, and Jose 1991). The two regions are separated by the yield stress, which is commonly interpreted by means of conventional graphical constructions implemented to the e–logσ' or log$e$–logσ' curve (e = void ratio and σ' = effective stress). Recently, the authors have proposed a subjective-free framework for determination of the yield stress with respect to four common graphical constructions, i.e., the maximum curvature method (Casagrande 1936), the Silva method (Pacheco Silva 1970), the recompression line–virgin compression line (RCL–VCL)

FIG. 6

Variations of the (a) primary and (b) secondary swelling rates against rubber content for the tested specimens.

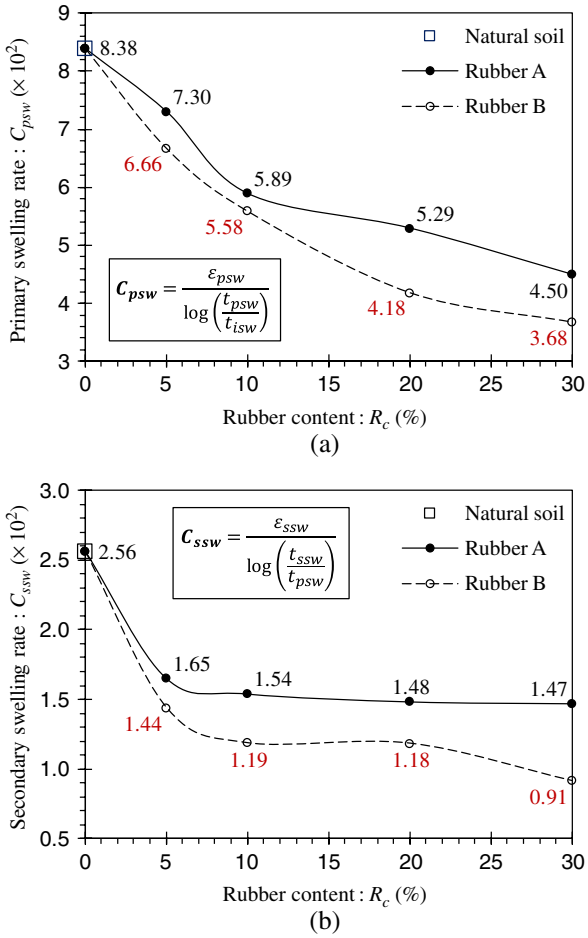

intercept method, and the log–log method (Jose, Sridharan, and Abraham 1989; Sridharan, Abraham, and Jose 1991). Adopting the proposed framework in Soltani et al. (2018), the average of the four graphical constructions was calculated for each specimen, and the results are provided in the form of yield stress paths in Fig. 7. Rubber reinforcement led to a slight increase in the yield stress. Natural soil exhibited a yield stress of $\sigma'_y = 17.73$ kPa. Maximum increase in σ'_y was observed in the case of 30 % rubber inclusion, which resulted in $\sigma'_y = 23.42$ and 22.10 kPa for Rubbers A and B, respectively.

Fig. 8a and b illustrates the variations of the compression index C_c (= slope of the VCL in Fig. 4b) and the swell index C_s (= slope of the unloading Path $B_1 \rightarrow C$ in Fig. 4b) against rubber content for the tested specimens, respectively. The rubber inclusions led to a noticeable reduction in C_c and C_s, indicating a capacity of counteracting material collapse when stressed. The greater the rubber content, the lower the C_c and C_s values following a monotonic trend. Rubber B often outperformed Rubber A in terms of lower C_c values. Regarding C_s, however, the performance of both rubber types seemed to be on par with each other. The natural soil resulted in $C_c = 0.249$ and $C_s = 0.136$. As a typical case, these values, respectively, dropped to 0.191 and 0.087 for Rubber A, and 0.187 and 0.078 for Rubber B, where $R_c = 20$ %.

FIG. 7

Void ratio–effective stress consolidation curves for the natural soil and various soil–rubber composites: (a) Rubber A and (b) Rubber B.

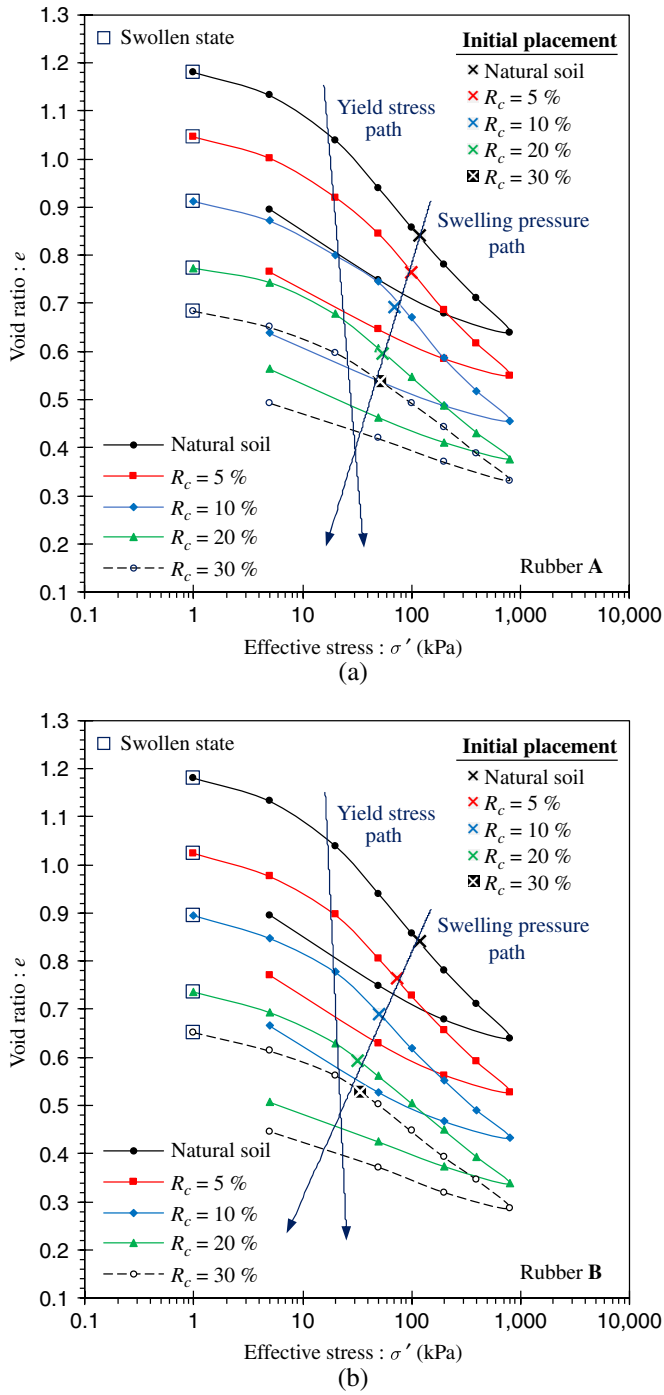

Rubber reinforcement altered the void ratio–effective stress locus, resulting in a major downward shift over the e:logσ' space. As a result, major variations were observed in the swelling pressure (see the swelling pressure paths in Fig. 7). Fig. 9 illustrates the variations

FIG. 8

Variations of the (a) compression and (b) swell indexes against rubber content for the tested specimens.

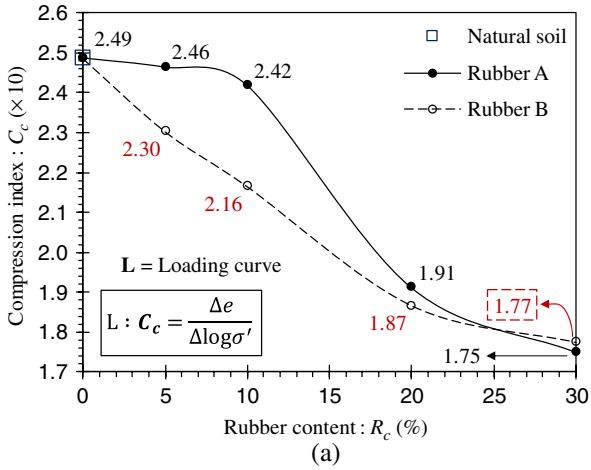

FIG. 9

Variations of swelling pressure and swelling potential against rubber content for the tested specimens.

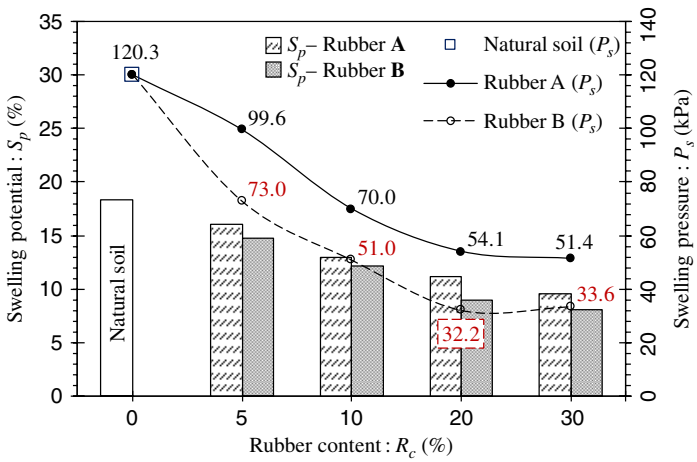

of swelling pressure and swelling potential against rubber content for the tested specimens. The variations of swelling pressure P_s followed a trend quite similar to that of swelling potential S_p, indicating that the greater the rubber content, the greater the decrease in S_p and P_s. For P_s, however, $R_c = 30$ % promoted similar results to $R_c = 20$ % with marginal differences, indicating that a maximum rubber inclusion of 20 % is sufficient to counteract the swelling properties. Similar to S_p, soil–Rubber B mixtures consistently outperformed similar specimens reinforced with Rubber A. The natural soil and soil–rubber mixtures corresponding to $R_c = 5$, 10, 20, and 30 % resulted in $P_s = 120.3$, 99.6, 70.0, 54.1, and 51.4 kPa, respectively. With Rubber B, these values dropped to $P_s = 73.0$, 51.0, 32.2, and 33.6 kPa, respectively.

The secondary consolidation characteristics were studied under an effective stress of $\sigma' = 50$ kPa, and the results are provided in Fig. 10. The completion time of the primary consolidation stage t_{pc} decreased because of the inclusion of Rubber A (see Fig. 10a). This effect, however, was less apparent for specimens reinforced with Rubber B, which essentially did not deviate t_{pc} (see Fig. 10b). The secondary consolidation rate C_{sc} can be defined as follows:

$$C_{sc} = \frac{\Delta \varepsilon_c}{\Delta \log t}\Bigg]_{t_{pc}}^{t_{sc}} = \frac{\varepsilon_{sc}}{\log\left(\frac{t_{sc}}{t_{pc}}\right)} \tag{3}$$

where $\varepsilon_c(t)$ = compression strain with respect to elapsed time t; ε_{sc} = secondary consolidation strain; and t_{sc} = completion time of the secondary consolidation stage (= 24 hours).

As a result of rubber reinforcement, the secondary consolidation rate exhibited a noticeable decreasing trend, indicating a capacity to counteract the settlement in both magnitude and time. The natural soil resulted in $C_{sc} = 7.28 \times 10^{-3}$. Where reinforced with 5, 10, 20, and 30 % Rubber A, C_{sc} dropped to 6.05×10^{-3}, 5.57×10^{-3}, 5.34×10^{-3}, and 5.02×10^{-3}, respectively. Similar inclusions of Rubber B, however, promoted slightly greater values, while still maintaining a noticeable advantage over the natural soil. In this case, $R_c = 5$, 10, 20, and 30 % resulted in $C_{sc} = 6.74 \times 10^{-3}$, 6.68×10^{-3}, 5.88×10^{-3}, and 4.94×10^{-3}, respectively. It is noteworthy to cross check the resulting trends for C_{sc} with C_{ssw}, which are expected to be somewhat consistent and comparable (Sridharan and Gurtug 2004; Phanikumar and Singla 2016).

EFFECT OF RUBBERS ON THE SHRINKAGE POTENTIAL

Void ratio–water content shrinkage curves, represented by the four-parameter logistic function (e.g., McGarry and Malafant 1987; Peng and Horn 2005; Thyagaraj, Thomas, and Das 2017), along with corresponding $Sr = 100$ % saturation lines, for the natural soil and various soil–rubber composites, are provided in Fig. 11a and b for Rubbers A and B, respectively. The four-parameter logistic function can be given as follows:

$$e(\omega) = e_{rsh} + \frac{e_{ssw} - e_{rsh}}{1 + \left(\frac{\omega}{\alpha}\right)^{-\beta}} \tag{4}$$

where e_{ssw} = void ratio at the swollen state A (i.e., the end of secondary swelling, as shown in Fig. 4c); e_{rsh} = void ratio at the fully desiccated state B_2 (see Fig. 4c); and α and β = fitting parameters (α and $\beta > 0$).

Similar to the swell path, a typical shrink path (see Path O→B_2 in Fig. 4c) develops into an *S*-shaped curve and thus can be divided into three regions, i.e., the structural,

FIG. 10

Secondary consolidation characteristics (under $\sigma' = 50$ kPa) for the natural soil and various soil–rubber composites: (a) Rubber A and (b) Rubber B.

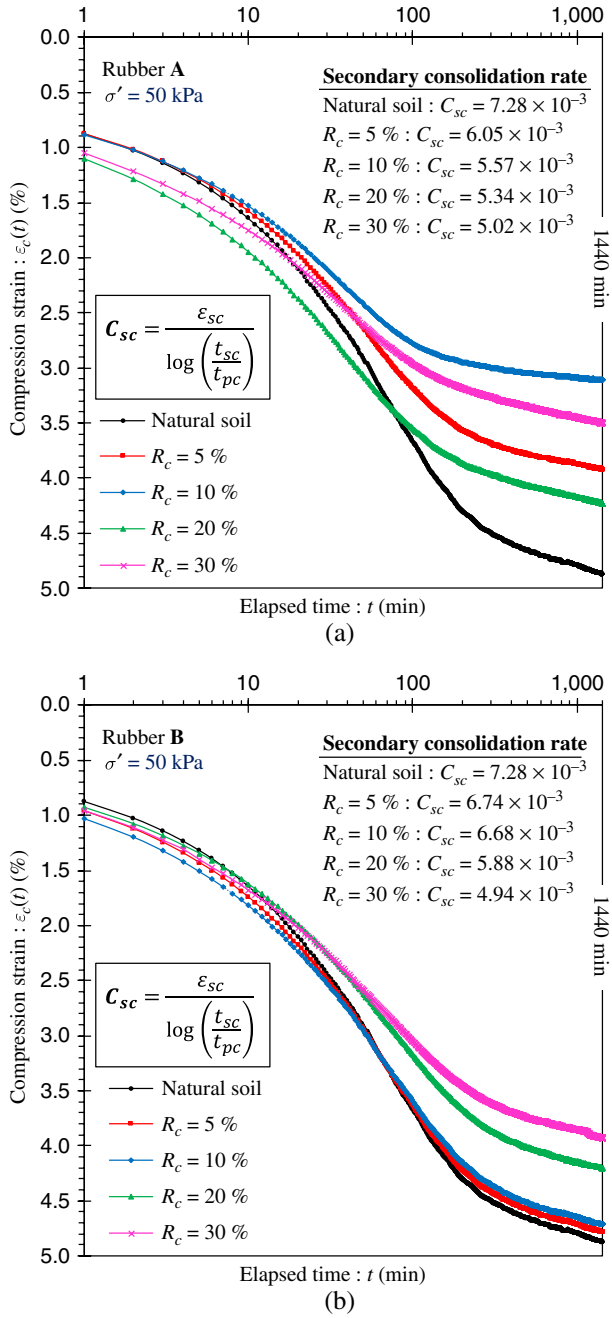

primary, and residual shrinkage, which are defined as phases during which shrinkage takes place (Haines 1923; Tripathy, Subba Rao, and Fredlund 2002; Cornelis et al. 2006; Estabragh, Moghadas, and Javadi 2013; Estabragh, Parsaei, and Javadi 2015). In the structural shrinkage phase, the decrease in volume of the soil is less than the volume of water lost from the stable void spaces. This portion of the shrinkage curve constitutes for small

FIG. 11

Void ratio–water content shrinkage curves for the natural soil and various soil–rubber composites: (a) Rubber A and (b) Rubber B.

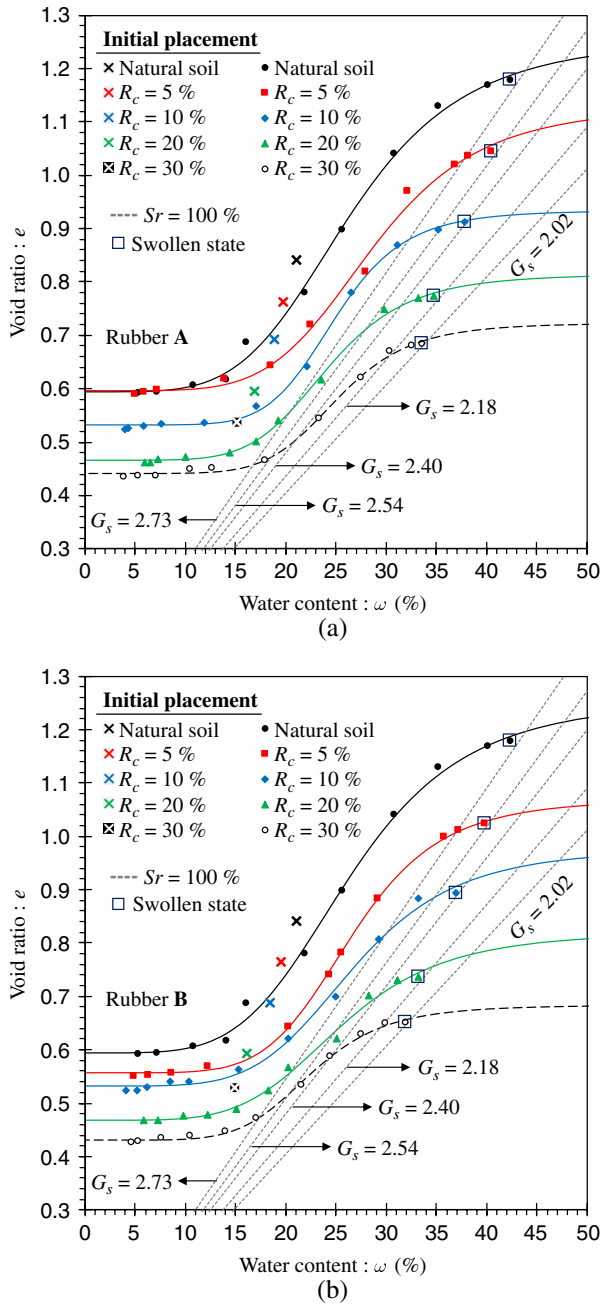

volume changes and is graphically represented by a mildly sloped curvilinear relationship. During primary shrinkage, also commonly referred to as normal shrinkage, the decrease in volume of the soil is essentially equal to the volume of lost water, thereby preventing the entrance of air into the soil pores. This portion of the shrinkage curve is represented by a steep sloped linear relationship, which is theoretically parallel to the $Sr = 100$ % saturation line. The primary shrinkage phase extends up to the shrinkage limit, which marks a

transitional state where the rate of volume change rapidly decreases, i.e., $\Delta e/\Delta\omega \rightarrow 0$. The majority of volume decrease takes place during the primary shrinkage phase. Completion of the primary shrinkage phase is further accompanied by residual shrinkage, where the entrance of air is allowed into the soil pores, thereby resulting in air-filled porosity. As a consequence of particles coming in contact, the decrease in volume of the soil becomes less than the volume of lost water. The magnitude of structural, primary, and residual shrinkage strains, i.e., ε_{ssh}, ε_{psh}, and ε_{rsh}, can be obtained by the following relationships (Mishra, Dhawan, and Rao 2008; Thyagaraj, Thomas, and Das 2017):

$$\varepsilon_{ssh} = \frac{\Delta e}{1 + e_{ssw}}\Bigg]_{e_{ssh}}^{e_{ssw}} = \frac{e_{ssw} - e_{ssh}}{1 + e_{ssw}} \tag{5}$$

$$\varepsilon_{psh} = \frac{\Delta e}{1 + e_{ssh}}\Bigg]_{e_{psh}}^{e_{ssh}} = \frac{e_{ssh} - e_{psh}}{1 + e_{ssh}} \tag{6}$$

$$\varepsilon_{rsh} = \frac{\Delta e}{1 + e_{psh}}\Bigg]_{e_{rsh}}^{e_{psh}} = \frac{e_{psh} - e_{rsh}}{1 + e_{psh}} \tag{7}$$

where, as outlined in **Fig. 4c**, e_{ssw} = void ratio at the swollen state A (i.e., the end of secondary swelling); e_{ssh} = void ratio at the end of structural shrinkage; e_{psh} = void ratio at the end of primary shrinkage (or at the shrinkage limit); and e_{rsh} = void ratio at the fully desiccated state B_2.

The total shrinkage strain, denoted as the shrinkage potential, can be defined as $SH_p = \varepsilon_{ssh} + \varepsilon_{psh} + \varepsilon_{rsh}$. The shrinkage strains and the shrinkage limit for the tested specimens are presented in **Table 5**. The shrinkage strains demonstrated a rubber content dependency, meaning that the greater the rubber content, the lower the shrinkage strains. The effect of rubber size, however, was observed to be marginal for the majority of cases. The shrinkage potential demonstrated a trend similar to that observed for the swelling potential. The natural soil displayed a shrinkage potential of $SH_p = 28.60$ %. Soil–Rubber A mixtures corresponding to $R_c = 5$, 10, 20, and 30 % resulted in $SH_p = 23.44$, 21.30, 18.27, and 15.30 %, respectively. Similar inclusions of Rubber B promoted slightly lower values and were measured as $SH_p = 24.61$, 20.44, 16.01, and 14.04 %, respectively. As a result of rubber reinforcement, the shrinkage limit experienced a minor increase; however, the resulting variations were observed to be less dependent on rubber content and

TABLE 5

Shrinkage strains and the shrinkage limit for the tested specimens.

Rubber Type	R_c (%)	ε_{ssh} (%)	ε_{psh} (%)	ε_{rsh} (%)	SH_p (%)	SL (%)[a]
–	–	4.15	21.47	2.98	28.60	14.88
Rubber A	5	2.99	17.50	2.95	23.44	17.82
	10	3.07	15.53	2.71	21.30	18.00
	20	2.49	13.62	2.15	18.27	16.25
	30	2.01	11.24	2.06	15.30	17.86
Rubber B	5	3.54	18.16	2.92	24.61	17.67
	10	2.43	15.33	2.68	20.44	16.40
	20	1.83	12.33	1.85	16.01	15.16
	30	1.86	10.43	1.75	14.04	15.18

Note: [a]shrinkage limit.

rubber size. The shrinkage limit is primarily a result of the "packing phenomenon" (i.e., optimal packing of soil particles during drying), which in turn is governed by the grain size distribution of the soil. As the soil's gradation becomes more and more uniform/poor (reduced packing capacity), the shrinkage limit tends to increase (Sridharan and Prakash 1998). The rubber particles used in this study are both classified as SP sand (see Fig. 1). As such, the addition of the poorly graded rubber to the well-graded soil offsets the well-distributed gradation of the host soil and thus gives rise to higher shrinkage limits. Consequently, this mechanism is expected to be in line with rubber content. The greater the rubber content, the more uniform/poor the grain size distribution, and thus the higher the shrinkage limit.

EFFECT OF RUBBERS ON THE STRENGTH PROPERTIES

Stress–strain curves obtained from the UC tests for the natural soil and various soil–rubber composites are provided in Fig. 12a and b for Rubbers A and B, respectively. The natural soil displayed a peak strength of $q_u = 113$ kPa, while the inclusion of 5 % Rubbers A and B resulted in $q_u = 129$ and 142 kPa, respectively. With $R_c = 10$ %, q_u dropped to 128 kPa

FIG. 12

Stress–strain UC curves for the natural soil and various soil–rubber composites: (a) Rubber A and (b) Rubber B.

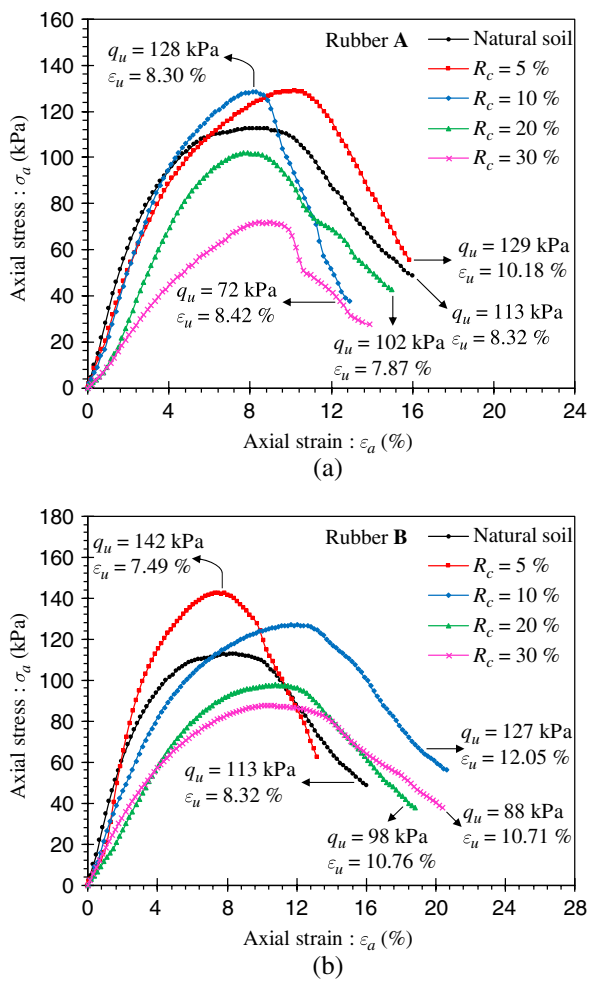

FIG. 13

Variations of strain energy at peak, and the peak strength against rubber content for the tested specimens.

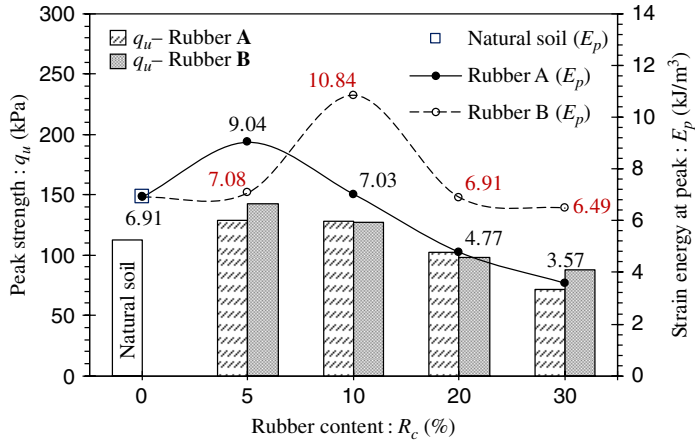

(for Rubber A) and 127 kPa (for Rubber B), which still maintains a noticeable advantage over the natural soil. Higher rubber inclusions, i.e., 20 and 30 %, however, gave rise to lower q_u values compared to that observed for the natural soil (i.e., $q_u = 102$ and 98 kPa for 20 % Rubbers A and B; and $q_u = 72$ and 88 kPa for 30 % Rubbers A and B). It is noteworthy to cross check q_u with S_p, P_s, and SH_p, which are in favor of a higher rubber content. This discrepancy implies that even though the rubbers are consistently effective at weaving the soil into a coherent matrix of restricted heave and settlement, when excessively included, they raise strength concerns.

Fig. 13 illustrates the variations of strain energy at peak E_p along with corresponding q_u values against rubber content for the tested specimens. The variations of E_p followed a trend quite similar to that observed for q_u. A noticeable improvement in the toughness can be achieved for rubber inclusions equal to or less than 10 %, while the higher rubber inclusions of 20 and 30 % gave rise to less toughness. Although in terms of q_u, the performance of both rubber types seemed to be on par with each other, soil–Rubber B mixtures consistently (with the exception of $R_c = 5$ %) promoted a higher toughness (i.e., higher E_p) compared to similar specimens reinforced with Rubber A. As optimum cases, E_p increased from 6.91 kJ/m^3 for the natural soil to 9.04 and 10.84 kJ/m^3 for the specimens reinforced with 5 % Rubber A and 10 % Rubber B, respectively. The elastic stiffness modulus E_{50}, defined as specimensthe secant modulus at 50 % of the peak strength (Radovic, Lara-Curzio, and Riester 2004; Iyengar et al. 2013), was also measured for the tested specimens. In general, the greater the rubber content, the lower the E_{50} value following a monotonic decreasing trend. Except for 5 % Rubber B, all specimens exhibited a lower E_{50} compared to the natural soil. The natural soil resulted in $E_{50} = 3.15$ MPa, while the inclusion of 5, 10, 20, and 30 % Rubber A resulted in $E_{50} = 2.47$, 2.56, 1.69, and 1.15 MPa, respectively. Similar inclusions of Rubber B did not significantly deviate from the aforementioned values (an exception was $R_c = 5$ %) and resulted in $E_{50} = 3.27$, 2.19, 1.45, and 1.59 MPa, respectively.

AMENDING MECHANISMS

Similar to fiber–reinforced soils, the rubber inclusions are able to amend the soil fabric through improvements achieved in three aspects, i.e., increase in nonexpansive fraction or

nonwetting attribute (Viswanadham, Phanikumar, and Mukherjee 2009a; Patil, Valdes, and Evans 2011; Trouzine, Bekhiti, and Asroun 2012; Estabragh, Rafatjo, and Javadi 2014; Soltani, Deng, and Taheri 2018), interlocking of rubber particles and soil grains (Tang et al. 2007, Tang, Shi, and Zhao 2010; Kalkan 2013; Phanikumar and Singla 2016; Soltani, Deng, and Taheri 2018), and frictional resistive forces generated as a result of soil–rubber contact (Cai et al. 2006; Al-Akhras et al. 2008; Viswanadham, Phanikumar, and Mukherjee 2009b; Patil, Valdes, and Evans 2011; Trouzine, Bekhiti, and Asroun 2012; Phanikumar and Singla 2016). The randomly distributed rubber particles resemble a spatial three-dimensional network in favor of weaving or interlocking the soil grains into a coherent matrix of restricted heave and settlement. The greater the number of included rubber particles, i.e., increase in rubber content, the more effective the interlocking effect. The frictional resistive forces grow as a consequence of rubber particles experiencing tensile/compressive stress in the presence of strong swelling/compression forces. Increases in rubber content leads to an increase in the total surface area, and thus a greater interfacial contact between rubber particles and soil grains. This in turn enhances the frictional effect between rubber particles, thereby mitigating the swell–shrink–consolidation capacity.

The swell–shrink–consolidation dependence on rubber size (or shape) is on par with the aspect ratio (i.e., fiber length-to-diameter ratio) in fiber–reinforced soils, and thus can be ascribed to the improvement mechanisms' interlocking and frictional resistive forces. Increase in rubber size increases the soil–rubber contact, which in turn generates a greater net frictional resistance between rubbers coupled with an enhanced soil–rubber interlocking effect. This improvement mechanism is also in line with rubber shape. As opposed to the granular form of Rubber A, the particles of Rubber B are relatively more fiber shaped (see **Fig. 2**); hence, they are more resilient to withstand (or translate) tensile/compressive stress along their axis, which, in turn, restricts the movement of soil particles interlocked to the rubber.

Optimum Rubber Content and Cost Analysis

The primary objective of any introduced stabilization scheme dealing with expansive soils should complement a decrease in the swell–shrink–consolidation capacity while either maintaining or improving the strength-related properties (Soltani 2017). Although both rubber types are consistently effective at weaving the soil into a coherent matrix of restricted heave and settlement (i.e., improvement in the swell–shrink–consolidation capacity is in favor of higher rubber contents), when excessively included they raise strength concerns. Based on the results presented in the first four sections under the "Results and Discussion" heading, a maximum rubber inclusion of 10 % seems to satisfy both objectives and thus can be deemed as the optimum choice. Where context changes and the strength and stiffness are not the primary concerns, higher rubber inclusions of up to 20 % may also be considered acceptable. The swell–shrink–consolidation properties were rubber size dependent, meaning that the rubber with a coarser size often outperformed the finer rubber. In terms of strength, however, the two rubber types promoted similar results with marginal differences. Therefore, the choice of rubber size would be dependent on design requirements/project objectives, rubber availability, and costs.

Table 6 summarizes a comparative cost analysis performed for the reinforcement of an assumed mass of 1,000 kg of soil using recycled tire rubbers and conventional polyester, polyethylene, or polypropylene fibers. The unit price for both rubber types and poly fibers

TABLE 6
Comparative cost analysis between rubbers and conventional fibers.

Type of Reinforcement	R_c (%)	f_c (%)[a]	Unit Price (AU$/kg)	Total Cost (AU$)
Rubber (A or B)	5	–	0.5	25.0
	10	–		50.0
	20	–		100.0
Poly- (ester, ethylene or propylene) fiber	–	0.8[b]	14.3	114.4
	–	1.5[c]		214.5

Note: [a]fiber content (i.e., fiber to dry soil mass ratio); [b]suggested by Olgun (2013) and Shahbazi et al. (2017); [c]suggested by Estabragh, Rafatjo, and Javadi (2014) and Soltani et al. (2017b).

were taken in accordance with common prices found in South Australian markets, which are approximately 0.5 and 14.3 AU$/kg, respectively. Other costs, such as transportation, labor, and compaction, have not been included as they are highly case and region dependent. Significant cost reduction can be achieved when rubbers are used as a replacement for conventional fibers. For instance, $R_c = 10$ % results in a total cost of 50 AU$, while the use of poly fibers at their so-called optimum contents, i.e., $f_c = 0.8$ and 1.5 %, results in 114.4 and 214.5 AU$, respectively. Unlike fibers, the rubber reinforcement technique requires a large quantity of rubber material to ameliorate the swell–shrink–consolidation capacity. However, in terms of total cost, it still maintains a significant advantage over conventional fibers. More importantly, beneficial reuse of recycled tires provides a sound environmental alternative to the safe disposal concern that is associated with such waste materials. The results of the cost analysis are in agreement with Yadav and Tiwari (2017), who carried out a similar comparative analysis with respect to the Indian market.

Conclusions

The following conclusions can be drawn from this study:

- As a result of rubber reinforcement, the swelling strain–time locus experienced a major downward shift over the semilog space, signifying a capacity to counteract the heave in both magnitude and time. Improvement in the rate and potential of swelling was dependent on both the rubber content and the rubber size, with the former taking on a more pronounced role. A similar dependency was also observed for the shrinkage potential. In this case, however, the effect of rubber size was observed to be marginal for the majority of cases.
- Rubber reinforcement altered the void ratio–effective stress consolidation locus, resulting in a significant reduction in the swelling pressure. The variations of swelling pressure suggested a trend similar to that of swelling potential. In addition, the rubber inclusions led to a noticeable reduction in the compression and swell indexes, indicating a capacity to counteract material collapse when stressed. The compression index was observed to be rubber size-dependent; however, for the swell index, the performance of both rubber types seemed to be on par with each other.
- The secondary consolidation rate also exhibited a rubber content/size dependency, indicating a capacity to counteract the settlement in both magnitude and time. The greater the rubber content, the lower the secondary consolidation rate, with the finer rubber maintaining a slight advantage over the coarser rubber. The resulting trends for the secondary swelling and secondary consolidation rates were observed to be consistent and comparable.

- The results of the UC tests were cross checked with the swell–shrink–consolidation properties to arrive at the optimum stabilization scenarios. A maximum rubber inclusion of 10 %, preferably the rubber of coarser category, proved to satisfy the stabilization objectives, and thus was deemed as the optimum choice. Where context changes and the strength and stiffness are not primary concerns, higher rubber inclusions of up to 20 % could also be considered acceptable.
- The cost efficiency of the rubber reinforcement technique was compared to conventional polyester, polyethylene, and polypropylene fibers. Significant cost reduction can be achieved when rubbers are used as a replacement for conventional fibers. More importantly, beneficial reuse of recycled tires provides a sound environmental alternative to the safe disposal concern associated with such waste materials.

ACKNOWLEDGMENTS

This research was funded by the Australian Research Council via project No. DP140103004, and their support is gratefully acknowledged.

References

Akbulut, S., Arasan, S., and Kalkan, E., 2007, "Modification of Clayey Soils Using Scrap Tire Rubber and Synthetic Fibers," *Appl. Clay Sci.*, Vol. 38, Nos. 1–2, pp. 23–32, https://doi.org/10.1016/J.CLAY.2007.02.001

Al-Akhras, N. M., Attom, M. F., Al-Akhras, K. M., and Malkawi, A. I. H., 2008, "Influence of Fibers on Swelling Properties of Clayey Soil," *Geosynth. Int.*, Vol. 15, No. 4, pp. 304–309, https://doi.org/10.1680/GEIN.2008.15.4.304

Alazigha, D. P., Indraratna, B., Vinod, J. S., and Ezeajugh, L. E., 2016, "The Swelling Behaviour of Lignosulfonate–Treated Expansive Soil," *Proc. ICE—Ground Improv.*, Vol. 169, No. 3, pp. 182–193, https://doi.org/10.1680/JGRIM.15.00002

Al-Rawas, A. A., Hago, A. W., and Al-Sarmi, H., 2005, "Effect of Lime, Cement and Sarooj (Artificial Pozzolan) on the Swelling Potential of an Expansive Soil from Oman," *Build. Environ.*, Vol. 40, No. 5, pp. 681–687, https://doi.org/10.1016/J.BUILDENV.2004.08.028

Ang, E. C. and Loehr, J. E., 2003, "Specimen Size Effects for Fiber–Reinforced Silty Clay in Unconfined Compression," *Geotech. Test. J.*, Vol. 26, No. 2, pp. 191–200, https://doi.org/10.1520/GTJ11320J

AS 1289.3.2.1:09, 2009, *Methods of Testing Soils for Engineering Purposes: Soil Classification Tests–Determination of the Plastic Limit of a Soil*, Standards Australia, Sydney, Australia, www.standards.org

AS 1289.3.3.1:09, 2009, *Methods of Testing Soils for Engineering Purposes: Soil Classification Tests–Calculation of the Plasticity Index of a Soil*, Standards Australia, Sydney, Australia, www.standards.org

AS 1289.3.9.1:15, 2015, *Methods of Testing Soils for Engineering Purposes: Soil Classification Tests–Determination of the Cone Liquid Limit of a Soil*, Standards Australia, Sydney, Australia, www.standards.org

ASTM D2166/D2166M-16, 2016, *Standard Test Method for Unconfined Compressive Strength of Cohesive Soil*, ASTM International, West Conshohocken, PA, www.astm.org

ASTM D2487-11, 2011, *Standard Practice for Classification of Soils for Engineering Purposes (Unified Soil Classification System)*, ASTM International, West Conshohocken, PA, www.astm.org

ASTM D422-63(2007)e2, 2007, *Standard Test Method for Particle–Size Analysis of Soils*, ASTM International, West Conshohocken, PA, www.astm.org

ASTM D427-04, 2004, *Test Method for Shrinkage Factors of Soils by the Mercury Method*, ASTM International, West Conshohocken, PA, www.astm.org

ASTM D4546-14, 2014, *Standard Test Methods for One–Dimensional Swell or Collapse of Soils*, ASTM International, West Conshohocken, PA, www.astm.org

ASTM D698-12e2, 2012, *Standard Test Methods for Laboratory Compaction Characteristics of Soil Using Standard Effort (12,400 ft–lbf/ft^3 (600 kN–m/m^3))*, ASTM International, West Conshohocken, PA, www.astm.org

ASTM D854-14, 2014, *Standard Test Methods for Specific Gravity of Soil Solids by Water Pycnometer*, ASTM International, West Conshohocken, PA, www.astm.org

Cai, Y., Shi, B., Ng, C. W. W., and Tang, C. S., 2006, "Effect of Polypropylene Fibre and Lime Admixture on Engineering Properties of Clayey Soil," *Eng. Geol.*, Vol. 87, Nos. 3–4, pp. 230–240, https://doi.org/10.1016/J.ENGGEO.2006.07.007

Casagrande, A., 1936, "The Determination of Pre–Consolidation Load and Its Practical Significance," *First International Conference on Soil Mechanics and Foundation Engineering*, A. Casagrande, P. C. Rutledge, and J. D. Watson, Eds., Harvard Printing Office, Cambridge, MA, pp. 60–64.

Cetin, H., Fener, M., and Gunaydin, O., 2006, "Geotechnical Properties of Tire–Cohesive Clayey Soil Mixtures as a Fill Material," *Eng. Geol.*, Vol. 88, Nos. 1–2, pp. 110–120, https://doi.org/10.1016/J.ENGGEO.2006.09.002

Cornelis, W. M., Corluy, J., Medina, H., Díaz, J., Hartmann, R., van Meirvenne, M., and Ruiz, M. E., 2006, "Measuring and Modelling the Soil Shrinkage Characteristic Curve," *Geoderma*, Vol. 137, Nos. 1–2, pp. 179–191, https://doi.org/10.1016/J.GEODERMA.2006.08.022

Dakshanamurthy, V., 1978, "A New Method to Predict Swelling Using Hyperbola Equation," *Geotech. Eng.*, Vol. 9, No. 1, pp. 29–38.

Dif, A. and Bluemel, W., 1991, "Expansive Soils under Cyclic Drying and Wetting," *Geotech. Test. J.*, Vol. 14, No. 1, pp. 96–102, https://doi.org/10.1520/GTJ10196J

Dunham-Friel, J. and Carraro, J. A. H., 2011, "Shear Strength and Stiffness of Expansive Soil and Rubber (ESR) Mixtures in Undrained Axisymmetric Compression," presented at the *Geo–Frontiers 2011: Advances in Geotechnical Engineering (GSP 211)*, Dallas, TX, American Society of Civil Engineers, Reston, VA, pp. 1111–1120.

Edil, T. and Bosscher, P., 1994, "Engineering Properties of Tire Chips and Soil Mixtures," *Geotech. Test. J.*, Vol. 17, No. 4, pp. 453–464, https://doi.org/10.1520/GTJ10306J

Estabragh, A. R., Moghadas, M., and Javadi, A. A., 2013, "Effect of Different Types of Wetting Fluids on the Behaviour of Expansive Soil during Wetting and Drying," *Soils Found.*, Vol. 53, No. 5, pp. 617–627, https://doi.org/10.1016/J.SANDF.2013.08.001

Estabragh, A. R., Parsaei, B., and Javadi, A. A., 2015, "Laboratory Investigation of the Effect of Cyclic Wetting and Drying on the Behaviour of an Expansive Soil," *Soils Found.*, Vol. 55, No. 2, pp. 304–314, https://doi.org/10.1016/J.SANDF.2015.02.007

Estabragh, A. R., Pereshkafti, M. R. S., Parsaei, B., and Javadi, A. A., 2013, "Stabilised Expansive Soil Behaviour during Wetting and Drying," *Int. J. Pavement Eng.*, Vol. 14, No. 4, pp. 418–427, https://doi.org/10.1080/10298436.2012.746688

Estabragh, A. R., Rafatjo, H., and Javadi, A. A., 2014, "Treatment of an Expansive Soil by Mechanical and Chemical Techniques," *Geosynth. Int.*, Vol. 21, No. 3, pp. 233–243, https://doi.org/10.1680/GEIN.14.00011

Estabragh, A. R., Soltani, A., and Javadi, A. A., 2016, "Models for Predicting the Seepage Velocity and Seepage Force in a Fiber Reinforced Silty Soil," *Comput. Geotech.*, Vol. 75, pp. 174–181, https://doi.org/10.1016/J.COMPGEO.2016.02.002

Fatahi, B., Khabbaz, H., and Fatahi, B., 2012, "Mechanical Characteristics of Soft Clay Treated with Fibre and Cement," *Geosynth. Int.*, Vol. 19, No. 3, pp. 252–262, https://doi.org/10.1680/GEIN.12.00012

Garcia, M., Pando, M. A., and Tempest, B., 2011, "Tire Derived Aggregates as a Sustainable Recycled Material for Retaining Wall Backfills," presented at the *International Conference on Sustainable Design and Construction* (ICSDC), Kansas City, MO, American Society of Civil Engineers, Reston, VA, pp. 542–552.

Gurtug, Y. and Sridharan, A., 2002, "Prediction of Compaction Characteristics of Fine–Grained Soils," *Géotechnique*, Vol. 52, No. 10, pp. 761–763, https://doi.org/10.1680/GEOT.2002.52.10.761

Gurtug, Y. and Sridharan, A., 2004, "Compaction Behaviour and Prediction of its Characteristics of Fine–Grained Soils with Particular Reference to Compaction Energy," *Soils Found.*, Vol. 44, No. 5, pp. 27–36, https://doi.org/10.3208/SANDF.44.5_27

Haines, W. B., 1923, "The Volume–Changes Associated with Variations of Water Content in Soil," *J. Agric. Sci.*, Vol. 13, No. 3, pp. 296–310, https://doi.org/10.1017/S0021859600003580

Hanafy, E. A. D. E., 1991, "Swelling/Shrinkage Characteristic Curve of Desiccated Expansive Clays," *Geotech. Test. J.*, Vol. 14, No. 2, pp. 206–211, https://doi.org/10.1520/GTJ10562J

Hannam, P., 2014, "Tyre Industry Divided over How to Handle Toxic Waste," The Sydney Morning Herald, Sydney, Australia, http://web.archive.org/web/20180623174900/https://www.smh.com.au/environment/tyre-industry-divided-over-how-to-handle-toxic-waste-20140120-314ic.html (accessed 23 June 2018).

Iyengar, S. R., Masad, E., Rodriguez, A. K., Bazzi, H. S., Little, D., and Hanley, H. J. M., 2013, "Pavement Subgrade Stabilization Using Polymers: Characterization and Performance," *J. Mater. Civ. Eng.*, Vol. 25, No. 4, pp. 472–483, https://doi.org/10.1061/(ASCE)MT.1943-5533.0000612

Jha, A. K. and Sivapullaiah, P. V., 2016, "Gypsum-Induced Volume Change Behavior of Stabilized Expansive Soil with Fly Ash-Lime," *Geotech. Test. J.*, Vol. 39, No. 3, pp. 391–406, https://doi.org/10.1520/GTJ20150017

Jones, L. D. and Jefferson, I., 2012, "Expansive Soils," *ICE Manual of Geotechnical Engineering: Volume I*, J. Burland, T. Chapman, M. Brown, and H. Skinner, Eds., Institution of Civil Engineers Publishing, London, UK, pp. 413–441.

Jose, B. T., Sridharan, A., and Abraham, B. M., 1989, "Log–Log Method for Determination of Preconsolidation Pressure," *Geotech. Test. J.*, Vol. 12, No. 3, pp. 230–237, https://doi.org/10.1520/GTJ10974J

Kalkan, E., 2013, "Preparation of Scrap Tire Rubber Fiber–Silica Fume Mixtures for Modification of Clayey Soils," *Appl. Clay Sci.*, Vols. 80–81, pp. 117–125, https://doi.org/10.1016/J.CLAY.2013.06.014

Maher, M. H. and Ho, Y. C., 1994, "Mechanical Properties of Kaolinite/Fiber Soil Composite," *J. Geotech. Eng.*, Vol. 120, No. 8, pp. 1381–1393, https://doi.org/10.1061/(ASCE)0733-9410(1994)120:8(1381)

McGarry, D. and Malafant, K. W. J., 1987, "The Analysis of Volume Change in Unconfined Units of Soil," *Soil Sci. Soc. Am. J.*, Vol. 51, No. 2, pp. 290–297, https://doi.org/10.2136/SSSAJ1987.03615995005100020059X

Mirzababaei, M., Arulrajah, A., Horpibulsuk, S., and Aldava, M., 2017, "Shear Strength of a Fibre-Reinforced Clay at Large Shear Displacement When Subjected to Different Stress Histories," *Geotext. Geomembr.*, Vol. 45, No. 5, pp. 422–429, https://doi.org/10.1016/J.GEOTEXMEM.2017.06.002

Mirzababaei, M., Miraftab, M., Mohamed, M., and McMahon, P., 2013a, "Impact of Carpet Waste Fibre Addition on Swelling Properties of Compacted Clays," *Geotech. Geol. Eng.*, Vol. 31, No. 1, pp. 173–182, https://doi.org/10.1007/S10706-012-9578-2

Mirzababaei, M., Miraftab, M., Mohamed, M., and McMahon, P., 2013b, "Unconfined Compression Strength of Reinforced Clays with Carpet Waste Fibers," *J. Geotech. Geoenviron. Eng.*, Vol. 139, No. 3, pp. 483–493, https://doi.org/10.1061/(ASCE)GT.1943-5606.0000792

Mirzababaei, M., Mohamed, M., Arulrajah, A., Horpibulsuk, S., and Anggraini, V., 2018, "Practical Approach to Predict the Shear Strength of Fibre–Reinforced Clay," *Geosynth. Int.*, Vol. 25, No. 1, https://doi.org/10.1680/JGEIN.17.00033

Mirzababaei, M., Yasrobi, S. S., and Al-Rawas, A. A., 2009, "Effect of Polymers on Swelling Potential of Expansive Soils," *Proc. ICE—Ground Improv.*, Vol. 162, No. 3, pp. 111–119, https://doi.org/10.1680/GRIM.2009.162.3.111

Mishra, A. K., Dhawan, S., and Rao, S. M., 2008, "Analysis of Swelling and Shrinkage Behavior of Compacted Clays," *Geotech. Geol. Eng.*, Vol. 26, No. 3, pp. 289–298, https://doi.org/10.1007/S10706-007-9165-0

Nalbantoglu, Z., 2006, "Lime Stabilization of Expansive Clay," *Expansive Soils: Recent Advances in Characterization and Treatment*, A. A. Al-Rawas and M. F. A. Goosen, Eds., Taylor & Francis Group, London, UK, pp. 139–148.

Olgun, M., 2013, "The Effects and Optimization of Additives for Expansive Clays under Freeze–Thaw Conditions," *Cold Reg. Sci. Technol.*, Vol. 93, pp. 36–46, https://doi.org/10.1016/J.COLDREGIONS.2013.06.001

Onyejekwe, S. and Ghataora, G. S., 2015, "Soil Stabilization Using Proprietary Liquid Chemical Stabilizers: Sulphonated Oil and a Polymer," *Bull. Eng. Geol. Environ.*, Vol. 74, No. 2, pp. 651–665, https://doi.org/10.1007/S10064-014-0667-8

Özkul, Z. and Baykal, G., 2007, "Shear Behavior of Compacted Rubber Fiber–Clay Composite in Drained and Undrained Loading," *J. Geotech. Geoenviron. Eng.*, Vol. 133, No. 7, pp. 767–781, https://doi.org/10.1061/(ASCE)1090-0241(2007)133:7(767)

Pacheco Silva, F., 1970, "A New Graphical Construction for Determination of the Preconsolidation Stress of a Soil Sample," presented at the *Fourth Brazilian Conference on Soil Mechanics and Foundation Engineering*, Vol. 2, No. 1, Rio de Janeiro, Brazil, pp. 225–232.

Patil, U., Valdes, J. R., and Evans, T. M., 2011, "Swell Mitigation with Granulated Tire Rubber," *J. Mater. Civ. Eng.*, Vol. 23, No. 5, pp. 721–727, https://doi.org/10.1061/(ASCE)MT.1943-5533.0000229

Peng, X. and Horn, R., 2005, "Modeling Soil Shrinkage Curve across a Wide Range of Soil Types," *Soil Sci. Soc. Am. J.*, Vol. 69, No. 3, pp. 584–592, https://doi.org/10.2136/SSSAJ2004.0146

Phanikumar, B. R. and Singla, R., 2016, "Swell–Consolidation Characteristics of Fibre-Reinforced Expansive Soils," *Soils Found.*, Vol. 56, No. 1, pp. 138–143, https://doi.org/10.1016/J.SANDF.2016.01.011

Prakash, K. and Sridharan, A., 2004, "Free Swell Ratio and Clay Mineralogy of Fine–Grained Soils," *Geotech. Test. J.*, Vol. 27, No. 2, pp. 220–225, https://doi.org/10.1520/GTJ10860

Radovic, M., Lara-Curzio, E., and Riester, L., 2004, "Comparison of Different Experimental Techniques for Determination of Elastic Properties of Solids," *Mater. Sci. Eng. A*, Vol. 368, Nos. 1–2, pp. 56–70, https://doi.org/10.1016/J.MSEA.2003.09.080

Rao, S. M., Thyagaraj, T., and Thomas, H. R., 2006, "Swelling of Compacted Clay under Osmotic Gradients," *Géotechnique*, Vol. 56, No. 10, pp. 707–713, https://doi.org/10.1680/GEOT.2006.56.10.707

Seda, J. H., Lee, J. C., and Carraro, J. A. H., 2007, "Beneficial Use of Waste Tire Rubber for Swelling Potential Mitigation in Expansive Soils," *Geo–Denver 2007: Soil Improvement (GSP 172)*, V. R. Schaefer, G. M. Filz, P. M. Gallagher, A. L. Sehn, and K. J. Wissmann, Eds., American Society of Civil Engineers, Reston, VA, pp. 1–9.

Shahbazi, M., Rowshanzamir, M., Abtahi, S. M., and Hejazi, S. M., 2017, "Optimization of Carpet Waste Fibers and Steel Slag Particles to Reinforce Expansive Soil Using Response Surface Methodology," *Appl. Clay Sci.*, Vol. 142, No. 15, pp. 185–192, https://doi.org/10.1016/J.CLAY.2016.11.027

Sibley, J. W. and Williams, D. J., 1989, "A Procedure for Determining Volumetric Shrinkage of an Unsaturated Soil," *Geotech. Test. J.*, Vol. 12, No. 3, pp. 181–187, https://doi.org/10.1520/GTJ10966J

Signes, C. H., Garzón-Roca, J., Fernández, P. M., Torre, M. E. G., and Franco, R. I., 2016, "Swelling Potential Reduction of Spanish Argillaceous Marlstone Facies Tap Soil through the Addition of Crumb Rubber Particles from Scrap Tyres," *Appl. Clay Sci.*, Vols. 132-133, pp. 768–773, https://doi.org/10.1016/J.CLAY.2016.07.027

Sivapullaiah, P. V., Sridharan, A., and Stalin, V. K., 1996, "Swelling Behaviour of Soil–Bentonite Mixtures," *Can. Geotech. J.*, Vol. 33, No. 5, pp. 808–814, https://doi.org/10.1139/T96-106-326

Soltani, A., 2017, "Discussion of 'Optimization of Carpet Waste Fibers and Steel Slag Particles to Reinforce Expansive Soil Using Response Surface Methodology' by M. Shahbazi, M. Rowshanzamir, S.M. Abtahi, S.M. Hejazi [Appl. Clay Sci., doi:10.1016/j.clay.2016.11.027]," *Appl. Clay Sci.*, https://doi.org/10.1016/J.CLAY.2017.07.020 (in press).

Soltani, A., Deng, A., and Taheri, A., 2018, "Swell–Compression Characteristics of a Fiber–Reinforced Expansive Soil," *Geotext. Geomembr.*, Vol. 46, No. 2, https://doi.org/10.1016/J.GEOTEXMEM.2017.11.009

Soltani, A., Deng, A., Taheri, A., and Mirzababaei, M., 2017a, "A Sulphonated Oil for Stabilisation of Expansive Soils," *Int. J. Pavement Eng.*, https://doi.org/10.1080/10298436.2017.1408270

Soltani, A., Deng, A., Taheri, A., Sridharan, A., and Estabragh, A. R., 2018, "A Framework for Interpretation of the Compressibility Behavior of Soils," *Geotech. Test. J.*, Vol. 41, No. 1, https://doi.org/10.1520/GTJ20170088

Soltani, A., Taheri, A., Khatibi, M., and Estabragh, A. R., 2017b, "Swelling Potential of a Stabilized Expansive Soil: A Comparative Experimental Study," *Geotech. Geol. Eng.*, Vol. 35, No. 4, pp. 1717–1744, https://doi.org/10.1007/S10706-017-0204-1

Sridharan, A., Abraham, B. M., and Jose, B. T., 1991, "Improved Technique for Estimation of Preconsolidation Pressure," *Géotechnique*, Vol. 41, No. 2, pp. 263–268, https://doi.org/10.1680/GEOT.1991.41.2.263

Sridharan, A. and Gurtug, Y., 2004, "Swelling Behaviour of Compacted Fine–Grained Soils," *Eng. Geol.*, Vol. 72, Nos. 1–2, pp. 9–18, https://doi.org/10.1016/S0013-7952(03)00161-3

Sridharan, A. and Nagaraj, H. B., 2005, "Plastic Limit and Compaction Characteristics of Fine–Grained Soils," *Proc. ICE—Ground Improv.*, Vol. 9, No. 1, pp. 17–22, https://doi.org/10.1680/GRIM.2005.9.1.17

Sridharan, A. and Prakash, K., 1998, "Mechanism Controlling the Shrinkage Limit of Soils," *Geotech. Test. J.*, Vol. 21, No. 3, pp. 240–250, https://doi.org/10.1520/GTJ10897J

Sridharan, A., Rao, A., and Sivapullaiah, P., 1986, "Swelling Pressure of Clays," *Geotech. Test. J.*, Vol. 9, No. 1, pp. 24–33, https://doi.org/10.1520/GTJ10608J

Srivastava, A., Pandey, S., and Rana, J., 2014, "Use of Shredded Tyre Waste in Improving the Geotechnical Properties of Expansive Black Cotton Soil," *Geomech. Geoeng.*, Vol. 9, No. 4, pp. 303–311, https://doi.org/10.1080/17486025.2014.902121

Subba Rao, K. S., Rao, S. M., and Gangadhara, S., 2000, "Swelling Behavior of a Desiccated Clay," *Geotech. Test. J.*, Vol. 23, No. 2, pp. 193–198, https://doi.org/10.1520/GTJ11043J

Tang, C. S., Shi, B., and Zhao, L. Z., 2010, "Interfacial Shear Strength of Fiber Reinforced Soil," *Geotext. Geomembr.*, Vol. 28, No. 1, pp. 54–62, https://doi.org/10.1016/J.GEOTEXMEM.2009.10.001

Tang, C. S., Shi, B., Gao, W., Chen, F., and Cai, Y., 2007, "Strength and Mechanical Behavior of Short Polypropylene Fiber Reinforced and Cement Stabilized Clayey Soil," *Geotext. Geomembr.*, Vol. 25, No. 3, pp. 194–202, https://doi.org/10.1016/J.GEOTEXMEM.2006.11.002

Thyagaraj, T. and Zodinsanga, S., 2014, "Swell–Shrink Behaviour of Lime Precipitation Treated Soil," *Proc. ICE—Ground Improv.*, Vol. 167, No. 4, pp. 260–273, https://doi.org/10.1680/GRIM.12.00028

Thyagaraj, T., Thomas, S. R., and Das, A. P., 2017, "Physico–Chemical Effects on Shrinkage Behavior of Compacted Expansive Clay," *Int. J. Geomech.*, Vol. 17, No. 2, 06016013, https://doi.org/10.1061/(ASCE)GM.1943-5622.0000698

Tripathy, S. and Subba Rao, K. S., 2009, "Cyclic Swell–Shrink Behaviour of a Compacted Expansive Soil," *Geotech. Geol. Eng.*, Vol. 27, No. 1, pp. 89–103, https://doi.org/10.1007/S10706-008-9214-3

Tripathy, S., Subba Rao, K. S., and Fredlund, D. G., 2002, "Water Content–Void Ratio Swell–Shrink Paths of Compacted Expansive Soils," *Can. Geotech. J.*, Vol. 39, No. 4, pp. 938–959, https://doi.org/10.1139/T02-022

Trouzine, H., Bekhiti, M., and Asroun, A., 2012, "Effects of Scrap Tyre Rubber Fibre on Swelling Behaviour of Two Clayey Soils in Algeria," *Geosynth. Int.*, Vol. 19, No. 2, pp. 124–132, https://doi.org/10.1680/GEIN.2012.19.2.124

Viswanadham, B. V. S., Phanikumar, B. R., and Mukherjee, R. V., 2009a, "Swelling Behaviour of a Geofiber–Reinforced Expansive Soil," *Geotext. Geomembr.*, Vol. 27, No. 1, pp. 73–76, https://doi.org/10.1016/J.GEOTEXMEM.2008.06.002

Viswanadham, B. V. S., Phanikumar, B. R., and Mukherjee, R. V., 2009b, "Effect of Polypropylene Tape Fibre Reinforcement on Swelling Behaviour of an Expansive Soil," *Geosynth. Int.*, Vol. 16, No. 5, pp. 393–401, https://doi.org/10.1680/GEIN.2009.16.5.393

Winterkorn, H. F. and Pamukcu, S., 1991, "Soil Stabilization and Grouting," *Foundation Engineering Handbook*, H. Y. Fang, Ed., Springer, New York, NY, pp. 317–378.

Yadav, J. S. and Tiwari, S. K., 2017, "A Study on the Potential Utilization of Crumb Rubber in Cement Treated Soft Clay," *J. Build. Eng.*, Vol. 9, pp. 177–191, https://doi.org/10.1016/J.JOBE.2017.01.001

Zornberg, J. G., Cabral, A. R., and Viratjandr, C., 2004, "Behaviour of Tire Shred–Sand Mixtures," *Can. Geotech. J.*, Vol. 41, No. 2, pp. 227–241, https://doi.org/10.1139/T03-086